Title
Neural innervation patterns in the sacral vertebral body

Journal
European Spine Journal, 25(6)

ISSN
0940-6719

Authors
Degmetich, Sean
Bailey, Jeannie F
Liebenberg, Ellen
et al.

Publication Date
2016-06-01

DOI
10.1007/s00586-015-4037-4

Peer reviewed

Published in final edited form as:

Eur Spine J. 2016 June ; 25(6): 1932–1938. doi:10.1007/s00586-015-4037-4.

Neural Innervation Patterns in the Sacral Vertebral Body

Sean Degmetich[1,2], **Jeannie F. Bailey**[1], **Ellen Liebenberg**[1], and **Jeffrey C. Lotz**[1]

[1]Department of Orthopaedic Surgery, University of California San Francisco, San Francisco, CA

[2]Relievant Medsystems, Inc., Redwood City, CA

Abstract

Purpose—Characterize the distribution of nerves within a single S1 vertebral body, with particular emphasis on the superior endplate that interfaces with the L5/S1 disc.

Methods—Musculature and connective tissue surrounding the sacrum was carefully dissected away for close visual inspection of penetrating nerve fibers. The S1 vertebral body was then isolated for histology and serial coronal sections were cut and stained with a ubiquitous neural antibody marker (PGP 9.5). Slides were analyzed and nerves were manually marked on high resolution, composite captured images, rendering 3D depictions of internal nerve distribution.

Results—The vast majority of nerves were closely associated with blood vessels within the marrow space with a uniform distribution in both the superior and inferior endplates of the S1 vertebral body. The highest nerve density was seen at the centrum (anatomic center) of the S1 vertebral body with smaller peaks seen at the lateral borders. Nerve fibers were observed branching from anterior sacral nerves and penetrating the lateral border of the S1 (during dissection), corresponding with peaks on nerve density maps.

Conclusions—Our results demonstrate that the S1 body and endplate are densely innervated and the peak in nerve density at the vertebral center coincides with vasculature patterns previously described in lumbar vertebral bodies. In the sacrum, however, there is no posterior nutrient foramen that facilitates nerve penetration through the vertebral cortex. Rather, our data indicate that nerves penetrate the S1 via the lateral aspects, consistent with being branches of the anterior sacral nerve. Since PGP 9.5 is a ubiquitous neural marker these identified nerves are likely composed of a mixed population of nociceptive and autonomic fibers.

Keywords

pain; nerve; vertebrae; sacroplasty; vertebroplasty; spine

INTRODUCTION

Chronic low back pain (CLBP) is a severe condition of the spinal column, with a lifetime prevalence of nearly 80% [1]. Up to 80% of CLBP cases are classified as non-specific, indicating that the pain-causing mechanism is unknown [2]. Yet nearly 40% of CLBP

Corresponding author: Jeffrey C. Lotz, 513 Parnassus Ave, 11th Floor S1157, San Francisco, CA 94143-0514, Tel: 415-476-7881, ; Email: Jeffrey.Lotz@ucsf.edu

coincides with disc degeneration [3]. Additionally, damage to the vertebral endplate is also suspected to be a common mechanism for disc degeneration [4, 5] since the bony vertebral endplate is innervated, and damage can lead a painful response [6]. While several studies on vertebral innervation focus on the lumbar spine [7–9], the S1 vertebrae may also be substantially affected by adjacent disc degeneration and is anatomically and functionally distinct from the lumbar vertebrae. Consequently, it is unclear how the origin and patterns of innervation of S1 compare to what is known for other lumbar bones. This is important since higher biomechanical loading at the L5-S1 intervertebral disc induces a greater degree of disc degeneration [10, 11], making surgical intervention at this site common. Therefore, the possibly distinct innervation patterns that accompany the unique S1 anatomy may be important for clinical management of patients with L5-S1 pathology.

Bone is an innervated source of pain [12, 13], making the vertebral body a candidate pain generator associated with adjacent disc degeneration [6, 7]. Evidence for endplate pain is supported by histologic studies demonstrating increased sensory nerve innervation at the endplate adjacent to degenerated discs [8, 9, 14], surgical reports demonstrating that the endplate is painful when touched [15, 16] and the positive association between Modic endplate abnormalities on MRI and the perception of pain [17, 18]. In further support of this, clinical studies indicate that vertebroplasty that disrupts vertebral innervation can alleviate pain [19], with similar findings reported for sacroplasty [20].

Presumably, the S1 innervation patterns would follow what already has been reported for lumbar vertebrae. Bailey [7] observed that nerves within L4 and L5 are associated with blood vessels and as such, the resulting distribution of nerves throughout the vertebral body follow historically established vascular patterns [21–26]. However, Bailey [7] also established that the primary origin of lumbar vertebrae innervation is the nutrient foramen on the posterior border, where lumbar arteries penetrate the cortex. Yet, since S1 is anatomically and functionally unique to the lumbar vertebrae, with the presence of the laterally adjacent large sacral nerves, the origin of innervation within S1 may significantly differ to that of the lumbar spine. Understanding S1 vertebral body innervation may help refine surgical methods and treatments involving the S1 vertebrae.

In this current study we sought to map the patterns of innervation within the S1 vertebral body. To accomplish this we stained serial histologic sections from a single S1 vertebral body using PGP 9.5, a pan-neural marker. PGP 9.5 is a pan-neural marker, not specific for nociceptive nerves, but it has been shown that the majority of PGP 9.5 positive nerves in bone and bone marrow also express markers for nociception [27]. The PGP 9.5 stained sections were then imaged and reconstructed in 3-dimensions so as to render the neural pattern. Using nerve density analysis and gross anatomic dissection, we define the origins and endpoints of nerves in S1.

MATERIALS AND METHDOS

Tissue Preparation and Histology

The S1 vertebral body used in this study came from a non-pathologic lumbosacral spine from a 42-year-old male within 72 hours post mortem (Willed Body Program, University of

California, San Francisco). The musculature and connective tissue surrounding the sacrum was carefully removed to minimize disruption of nerves penetrating the S1 vertebral body. For optimum tissue processing, the S1 was first cut into 4 equally spaced coronal slabs (approximately 7–9 mm thick) using a band saw. Each of the slabs was fixed in 10% neutral buffered formalin for 7 days. Specimens were then decalcified by ion exchange and confirmed by radiography. The slabs were then dehydrated with an ascending series of ethanol changes, cleared with Clearite, and embedded by paraffin infiltration. Serial coronal sections were cut 7um thick, and one section every 300 um was stained with a ubiquitous neural antibody marker (PGP 9.5) and counterstained with Mallory-Heidenhain to contrast marrow and trabecular elements. Nerves were identified using PGP 9.5 staining. PGP 9.5 was used because it stains well on paraffin histology and it had less artifact staining than other pan-neural markers (NF200). PGP 9.5 is a pan-neural marker that has shown to co-localize with CGRP, a nociceptive nerve marker [7].

Nerve quantification

A total of 45 stained histological sections were used in our analysis. High-resolution images of the stained sections were taken at 40× total magnification and tiled together using a motorized stage in conjunction with image analysis software (NewCAST, Visopharm, Horsholm, Denmark). Resulting composite images were equally sized (8064 × 8496 pixels) and aligned using the superior endplate and anterior sacral foramen as a guides. The composite images from each slide were analyzed microscopically at 100× total magnification. PGP 9.5 positive nerves were manually marked on an overlying layer (Figure 1). Then using image analysis software (Image J, NIH) we quantified the total pixel area of individual nerves within 81 equally sized (896 × 944 pixel) regions of interest (ROIs) gridded across each image. All 81 non-overlapping ROIs created a 9 × 9 grid covering the entire coronal section (Figure 2). Two-dimensional color maps of nerve density were generated using Matlab (The MathWorks, Inc., Natick, MA, USA) and used to visualize innervation patterns (Figure 3–5).

Investigative Gross Dissection

We harvested a second lumbosacral spine from a 50-year-old male within 48 hours post-mortem (Willed Body Program, University of California, San Francisco, CA). The musculature and connective tissue surrounding the sacrum was carefully dissected away without disrupting any free nerve roots or connective tissue associated with the sacrum. The bony wings that make up the lateral borders of the cranial sacrum were separated from the S1 through the sacral foramen. This allowed us to visualize the lateral borders of the S1 that makes up the medial border of the left and right anterior sacral foramen. The entire S1 was inspected for major sites of nerve entry.

RESULTS

Nerve Density

Transverse plane nerve maps showed a uniform nerve distribution at both the superior and inferior region of S1 adjacent to the endplate with the vast majority of area density at the center of the vertebral body (Figure 3). The central-most sections reveal a large isolated peak

in nerve area density at the vertebral centrum (anatomic center) with lesser peaks, nearly half as dense as the centrum, spanning the distance from the centrum to the lateral borders of the S1 vertebral body [FigB]. A similar pattern is shown between the centrum and the anterior border, however unlike the lateral borders, nerve presence ceases 10mm from the anterior border. The posterior region appears sparsely innervated, similar to the superior and inferior endplate regions [Fig 3B].

Coronal plane nerve maps support trends observed in the transverse plane maps. Differences include the position of density peak in the centrum, although there is a expansive zone of elevated nerve density through the central coronal plane, it appears the peak of density is located 5mm closer to the superior endplate (Figure 4B). Lastly, sagittal plane nerve maps also support trends found in both transverse and coronal planes, but with emphasis on elevated nerve density at the lateral borders (Figures 5A & 5C) and mid-sagittal distribution of nerve density showing a significant central peak that tappers toward the superior and inferior endplates (Figure 5B).

Investigative Gross Dissection

We observed evidence of a large plexus of nerves emanating from both the left and right branches of the anterior sacral nerve. These coursed into the lateral border of S1 as they passed through their respective left and right anterior sacral foramen. We did not observe any gross evidence of inter-body innervation in any other region of the S1 (Figure 6).

DISCUSSION

We sought to establish the innervation pattern of the human S1 vertebra. Results from the 3-dimensional distributions indicate that nerves are densely present at the mid-lateral borders of the S1 vertebral body, while not present at the mid-posterior border, suggesting the main point of entry for nerves is at the sacral foramen (Figure 6). S1 does have an apparent nutrient foramen on the posterior border, but the lack of nerves along the posterior border of the S1 vertebral body indicates that the neural anatomy is distinct from lumbar vertebra. On the other hand, once inside the S1 vertebral body, like L4/L5, the nerves form a large cluster in the center of the body then taper in the directions of the cranial and caudal endplates. This pattern follows already established vascularity trends of the lumbar vertebral bodies [21, 22, 25, 26].

Para-sagittal and mid-coronal distribution maps demonstrate clear peaks in the lateral borders of S1 [Figures 3, 4]. In addition gross dissection of a lumbosacral spine shows the presence of penetrating nerve fibers branching from the anterior sacral nerve at the same region [Figures 5, 6]. This suggests that fibers from the anterior sacral nerve may play a significant role in the contribution of nociceptive fibers to the vertebral centrum and endplate.

The S1 nerve root, seen depicted in [Figure 7], joins with the lumbosacral trunk (L4/L5) and S2/S3 nerve roots to form important motor and sensory structures of the pelvis and lower extremities. Patients who experience sciatica resulting from compression or disruption of the sciatic nerve or any of its supplying nerve roots often experience symptoms of CLBP. This

notion is clinically important for vertebrogenic pain, as we have demonstrated S1 sacral nerve roots as a likely source neural architecture in S1.

A limitation of our study is that nerves were identified using a pan-neural marker, PGP 9.5, that is not specific to pain fibers. However, we have previously demonstrated that within vertebra, PGP 9.5 co-localizes with calcitonin gene-related-peptide (CGRP), a known nociceptive marker [7]. CGRP immunohistochemistry is associated with high background staining, and consequently doesn't lend itself to three-dimensional mapping as we performed here. However, we expect that 80% of PGP 9.5-positive nerves in bone and bone marrow could express CGRP. A previous study, measuring the expression of TrkA in skeletal tissues demonstrated that TrkA is expressed in the majority of PGP 9.5 positive nerves in paraffin histology and in 80% of CGRP positive nerves in frozen histology [27]. Additionally, the presence of pain eliciting nerves within the S1 vertebral body is further supported by previous studies reporting pain alleviation following sacroplasty [20]. While the vast majority of nerves were observed adjacent to blood vessels, PGP 9.5 nerves were seen in all elements of our slides including marrow elements, cartilage, and bony structures. This further substantiates our claim that our PGP 9.5 stained nerves represent a mixed population of autonomic and nociceptive fibers.

Another limitation is the small sample size. Because of the large number of histology slides required for three-dimensional nerve mapping, and the method by which the nerve maps where identified manually, the sample size was limited to 1. However, our results are consistent with a previous study examining innervation patterns with a lumbar vertebra [7]. This notion is also supported by previous studies showing consistent distribution of nerves and blood vessels across donors [21, 22, 7].

In summary, S1 innervation by the anterior sacral nerve has not been reported previously. Previous studies have shown the internal structure of lumbar vertebral bodies are innervated via nerves passing through the basivertebral foramen (a single posterior structure) [7]. This is in contrast to data we report here that indicates S1 innervation is via two points at the lateral/inferior vertebral borders, where branches from the anterior sacral nerve penetrate the vertebral cortex. Further investigation into these new potential sites of origin may provide therapeutic options for future procedures in spine surgery.

Acknowledgements

Funding provided by Relievant Medsystems, Inc.

References

1. Freburger JK, Holmes GM, Agans RP, et al. The rising prevalence of chronic low back pain. Arch Intern Med. 2009; 169(3):251–258. [PubMed: 19204216]
2. Balagué F, Mannion AF, Pellisé F, et al. Non-specific low back pain. Lancet. 2012; 379:482–491. [PubMed: 21982256]
3. Kallewaard JW, Terheggen MA, Groen GJ, et al. Discogenic Low Back Pain. Pain Pract. 2010; 10(6):560–579. 15. [PubMed: 20825564]

4. Kerttula LI, Serlo WS, Tervonen OA, et al. Post-Traumatic Findings of the Spine After Earlier Vertebral Fracture in Young Patients Clinical and MRI Study. Spine. 2000; 25(9):1104–1108. [PubMed: 10788855]
5. Adams MA. Biomechanics of back pain. Acupunct Med. 2004; 22(4):178–188. [PubMed: 15628775]
6. Lotz JC, Fields AJ, Liebenberg E. The role of the vertebral end plate in low back pain. Global Spine J. 2013; 3(3):153–164. [PubMed: 24436866]
7. Bailey JF, Liebenberg E, Degmetich S, et al. Innervation patterns of PGP 9.5-positive nerve fibers within the human lumbar vertebra. J Anat. 2011; 218(3):263–270. [PubMed: 21223256]
8. Brown MF, Hukkanen MV, McCarthy ID, et al. Sensory and sympathetic innervation of the vertebral endplate in patients with degenerative disc disease. J Bone Joint Surg Br. 1997; 79(1):147–153. [PubMed: 9020464]
9. Freemont AJ, Watkins A, Le Maitre C, et al. Nerve growth factor expression and innervation of the painful intervertebral disc. J Pathol. 2002; 197(3):286–292. [PubMed: 12115873]
10. Grant JP, Oxland TR, Dvorak MF, et al. The effects of bone density and disc degeneration on the structural property distributions in the lower lumbar vertebral endplates. J Orthop Res. 2002; 20(5):1115–1120. [PubMed: 12382980]
11. Keller TS, Colloca CJ, Harrison DE, et al. Influence of spine morphology on intervertebral disc loads and stresses in asymptomatic adults: implications for the ideal spine. Spine J. 2005; 5(3): 297–309. [PubMed: 15863086]
12. Serre CM, Farlay D, Delmas PD, et al. Evidence for a dense and intimate innervation of the bone tissue, including glutamate-containing fibers. Bone. 1991; 25(6):623–629. [PubMed: 10593406]
13. Mach DB, Rogers SD, Sabino MC, et al. Origins of skeletal pain: sensory and sympathetic innervation of the mouse femur. Neurosci. 2002; 113(1):155–166.
14. Fagan A, Orth F, Moore R, et al. ISSLS prize winner : The innervation of the intervertebral disc: a quantitative analysis. 2003; 28(23):2570–2576.
15. Peng B, Chen J, Kuang Z, et al. Diagnosis and surgical treatment of back pain originating from endplate. Euro Spine J. 2009; 18(7):1035–1040.
16. Kuslich SD, Ulstrom CL, Michael CJ. The tissue origin of low back pain and sciatica: a report of pain response to tissue stimulation during operations on the lumbar spine using local anesthesia. Orthop Clin North Am. 1991; 22:181–187. [PubMed: 1826546]
17. Weishaupt D, Zanetti M, Hodler J, et al. Painful lumbar disk derangement: relevance of endplate abnormalities at MR imaging. Radiology. 2001; 218(2):420–427. [PubMed: 11161156]
18. Modic MT, Masaryk TJ, Ross JS, et al. Imaging of degenerative disk diseases. Curr Opin Radiol. 1988; 4:103–114.
19. Niv D, Gofeld M, Devor M. Causes of pain in degenerative bone and joint disease: a lesson from vertebroplasty. Pain. 2003; 105(3):387–392. [PubMed: 14527699]
20. Dehdashti AR, Martin J, Jean B, et al. PMMA cementoplasty in symptomatic metastatic lesions of the S1 vertebral body Cardiovasc Intervent Radiol. 2000; 23:235–237.
21. Crock HV. The arterial supply and venous drainage of the vertebral column of the dog. J Anat. 1960; 94:88–99. [PubMed: 13812915]
22. Crock HV, Goldwasser M. Anatomic studies of the circulation in the region of the vertebral end-plate in adult Greyhound dogs. Spine. 1984; 9:702–706. [PubMed: 6505840]
23. Bogduk N, Long DM. Percutaneous lumbar medial branch neurotomy: a modification of facet denervation. Spine. 5:193–200. [PubMed: 6446163]
24. Bogduk N, Tynan W, Wilson S. The nerve supply to the human lumbar intervertebral discs. J Anat. 1981; 132:39–56. [PubMed: 7275791]
25. Ratcliffe JF. The arterial anatomy of the adult human lumbar vertebral body: a microarteriographic study. J Anat. 1980; 131:57–79. [PubMed: 7440404]
26. Ratcliffe JF. The arterial anatomy of the developing human dorsal and lumbar vertebral body: a microarteriographic study" (1981). J Anat. 1981; 133:625–638. [PubMed: 7333964]

27. Castaneda-Corral G, Jimenez-Andrade JM, Bloom AP, et al. The majority of myelinated and unmyelinated sensory nerve fibers that innervate bone express the tropomyosin receptor kinase A. Neurosci. 2011; 178:196–207.

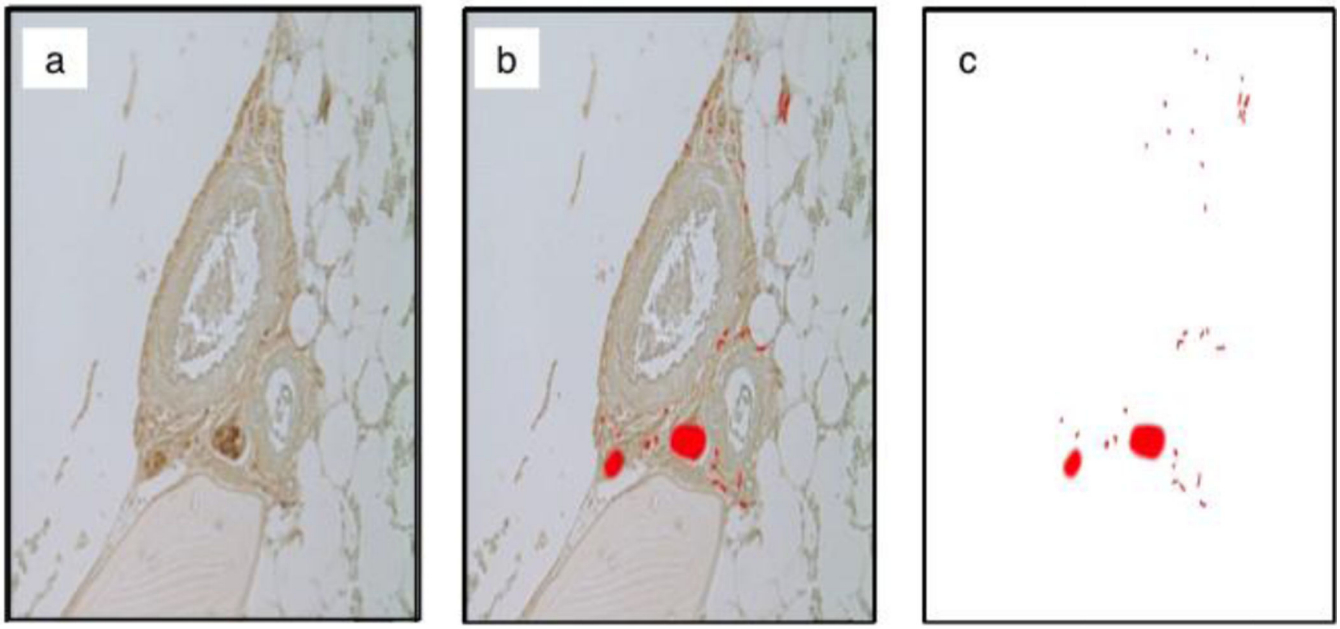

Figure 1.

Demonstrates the methodology used in identifying PGP 9.5 positive nerves. (a) Microscopic view of an unmarked histology image containing a vessel with surrounding neural elements. (b) Nerves on the image are manually marked on a blank overlying layer. (c) Background layer is removed leaving the marked binary layer available for image analysis.

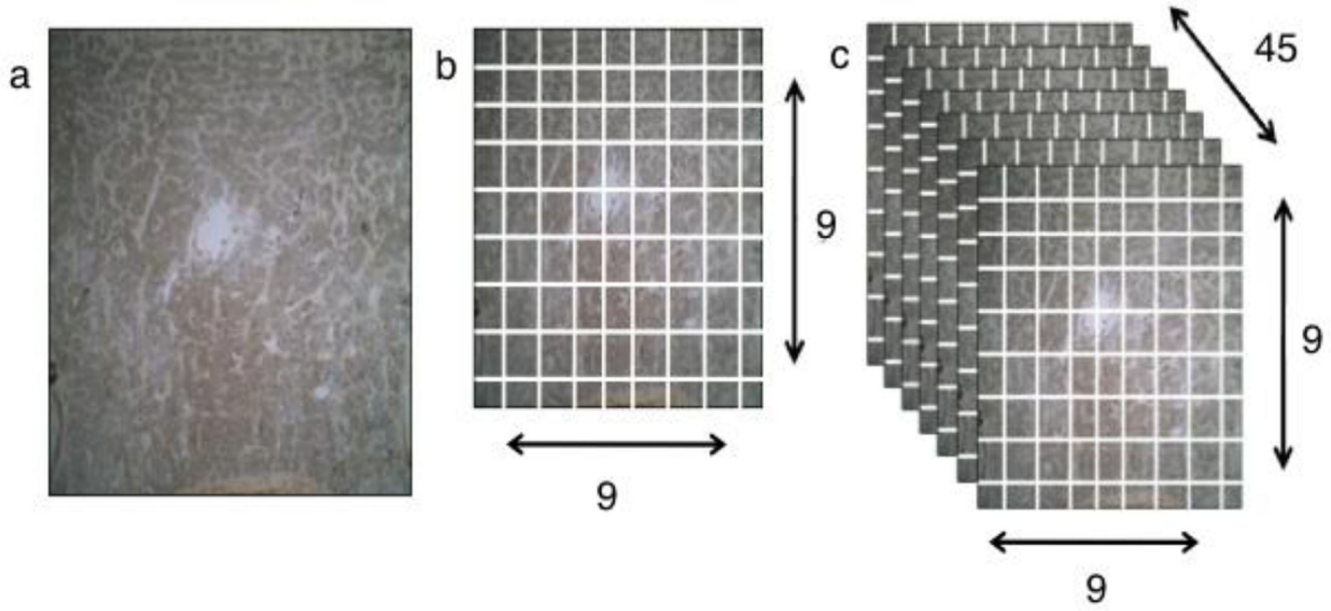

Figure 2.

Methodology used in quantifying the spatial distribution of PGP 9.5 positive nerves. (a) 40× total magnification view of a marked coronal slide. (b) Image is divided into 81 distinct ROI. (c) With 81 ROI per slide and 45 slides total, there was a total of 3,645 ROIs used in this study. The data were combined to form a single 3 dimensional rendering.

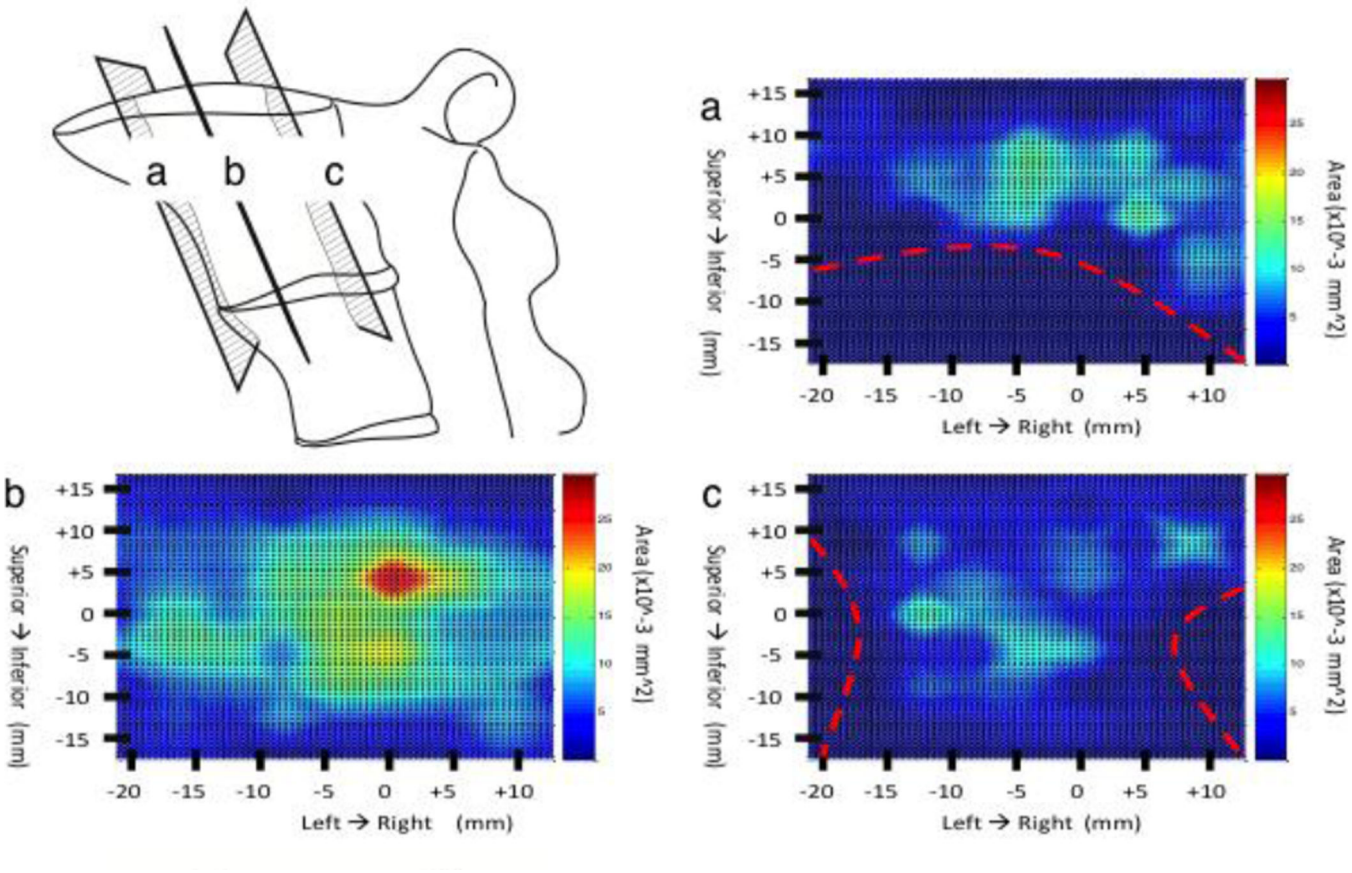

Figure 3.

Coronal view color maps of the nerve area density in the S1. Maps (a & b) represent coronal views near the anterior and posterior border respectively. Map B represents and a central coronal view approximately half way between the anterior and posterior vertebral surfaces. The red dashed lines shown in (a & c) represent boundary sites were no bone is present. The zero point on the x-axis represents the midpoint between the left and right boarders of the S1. The zero point on the y-axis represents the halfway point between the S1 superior and inferior EP.

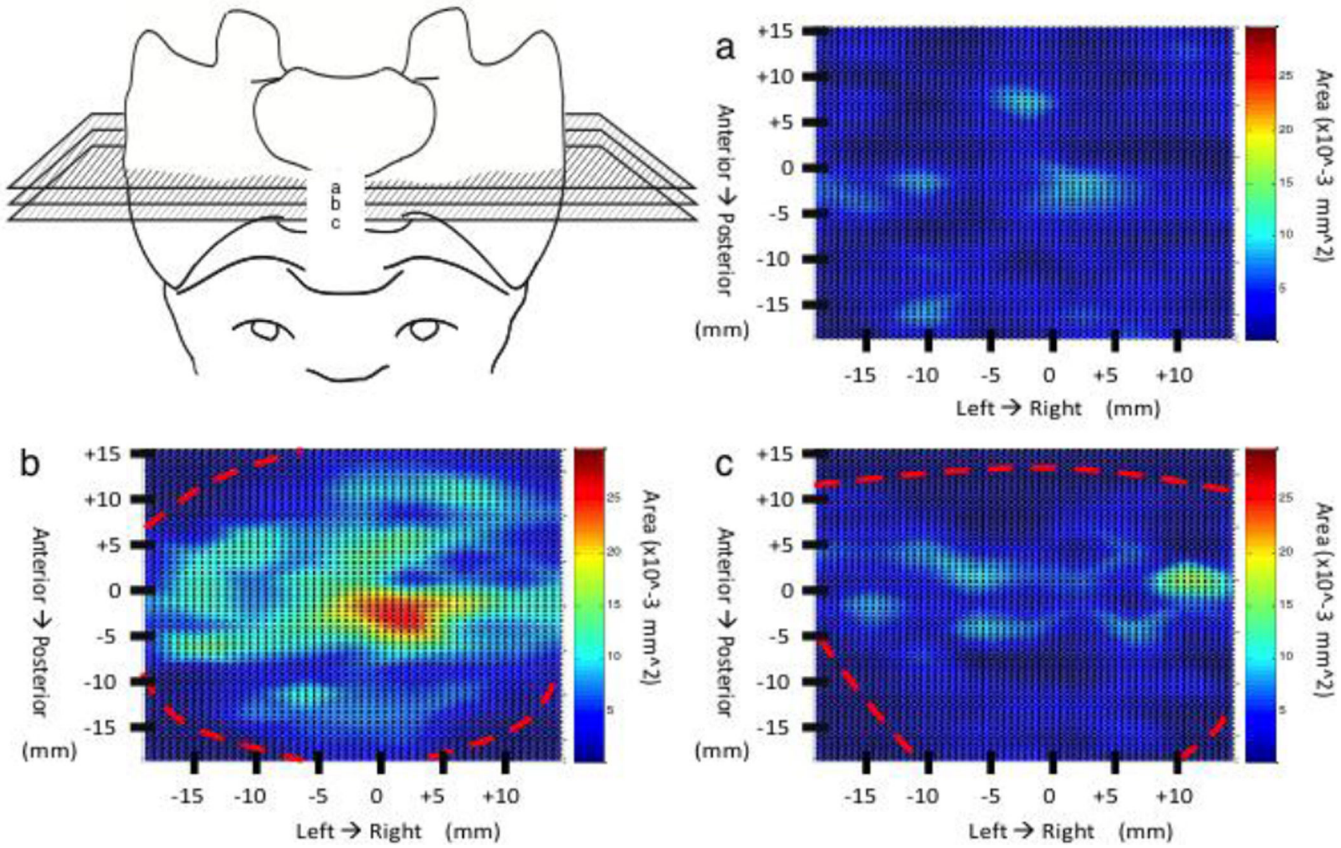

Figure 4.

Axial view color maps of the nerve area density in the S1. Maps (a & c) represent axial views near the superior and inferior EP respectively. Map B represents and a central axial view approximately half way between the superior and inferior EP. The red dashed lines shown in (b & c) represent boundary sites were no bone is present. The zero point on the x-axis represents the midpoint between the left and right borders of the S1. The zero point on the y-axis represents the halfway point between the anterior and posterior border of the S1 while running along the superior EP.

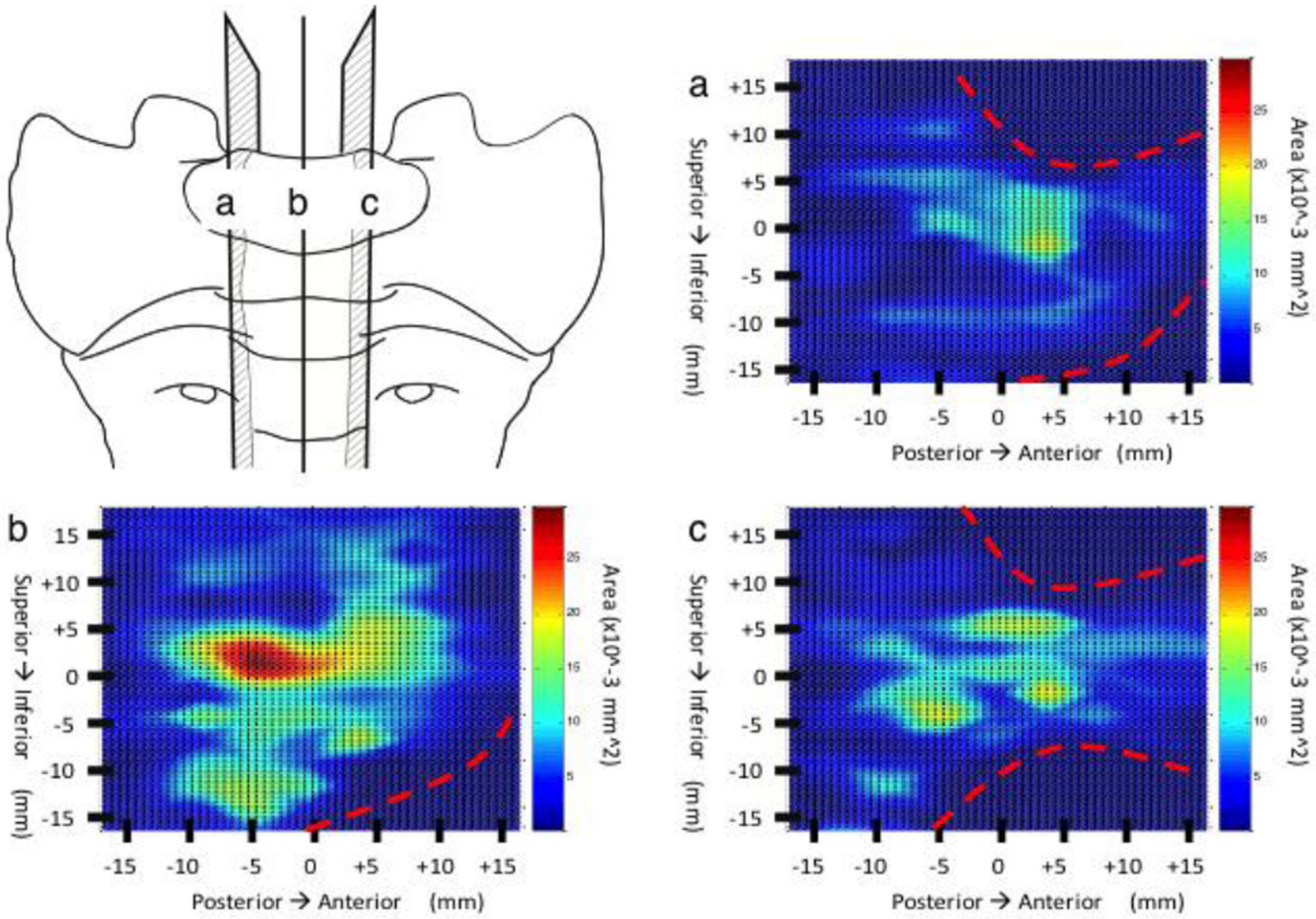

Figure 5.

Sagittal view color maps of the nerve area density in the S1. Maps (a & c) represent sagittal views near the left and right borders respectively. Map B represents and a central axial view approximately half way between the left and right borders. The red dashed lines shown in (a, b & c) represent boundary sites were no bone is present. The zero point on the x-axis represents the midpoint between the anterior and posterior borders of the S1. The zero point on the y-axis represents the halfway point between the S1 superior and inferior EP.

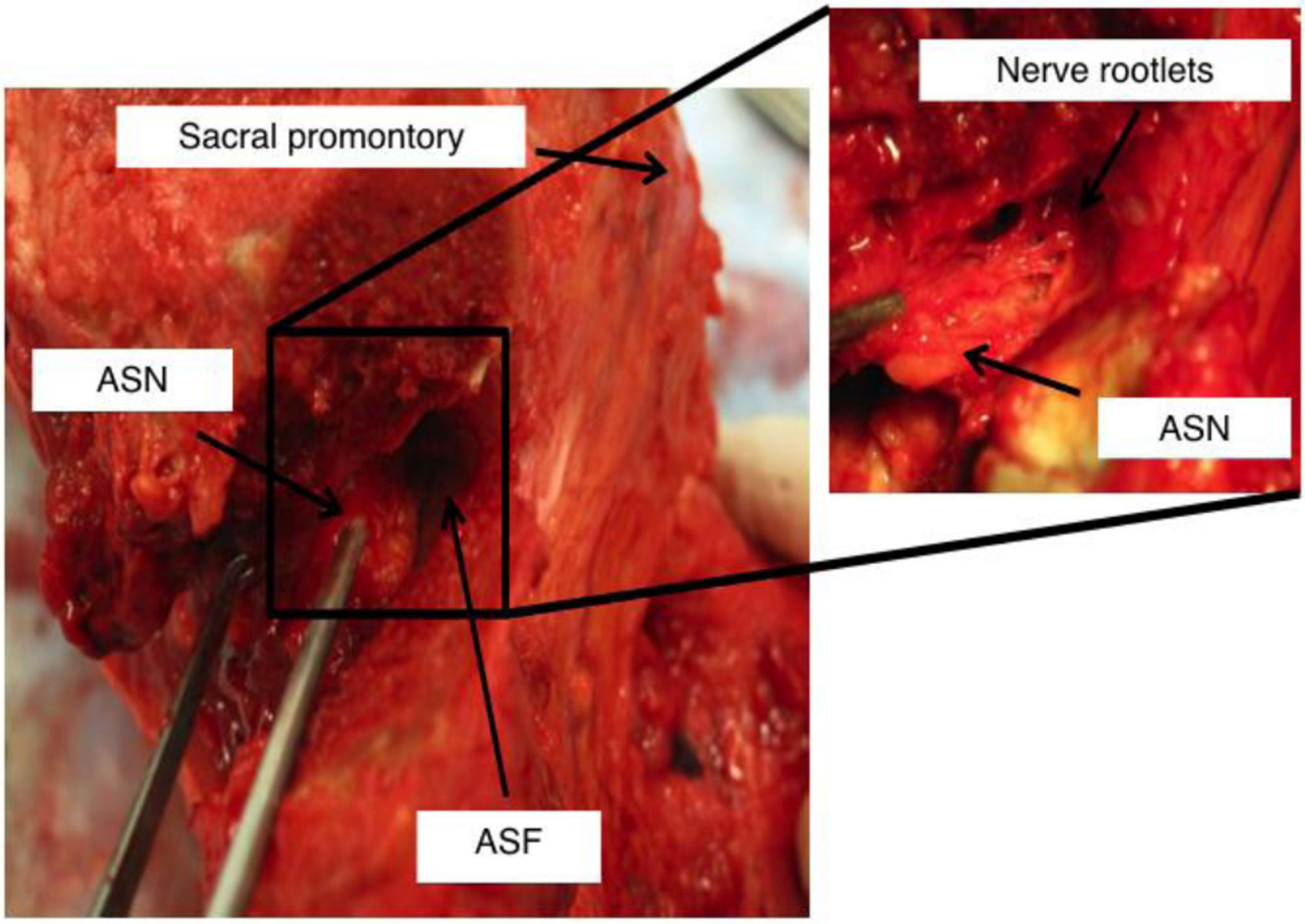

Figure 6.

Inferior-anterior view of a dissected S1 vertebral body. The bony lateral boarder of the anterior sacral foramen (ASF) has been removed exposing its normally hidden medial boarder. Nerve fibers are clearly seen branching from the anterior sacral nerve (ASN) leading into the sacral vertebral body.

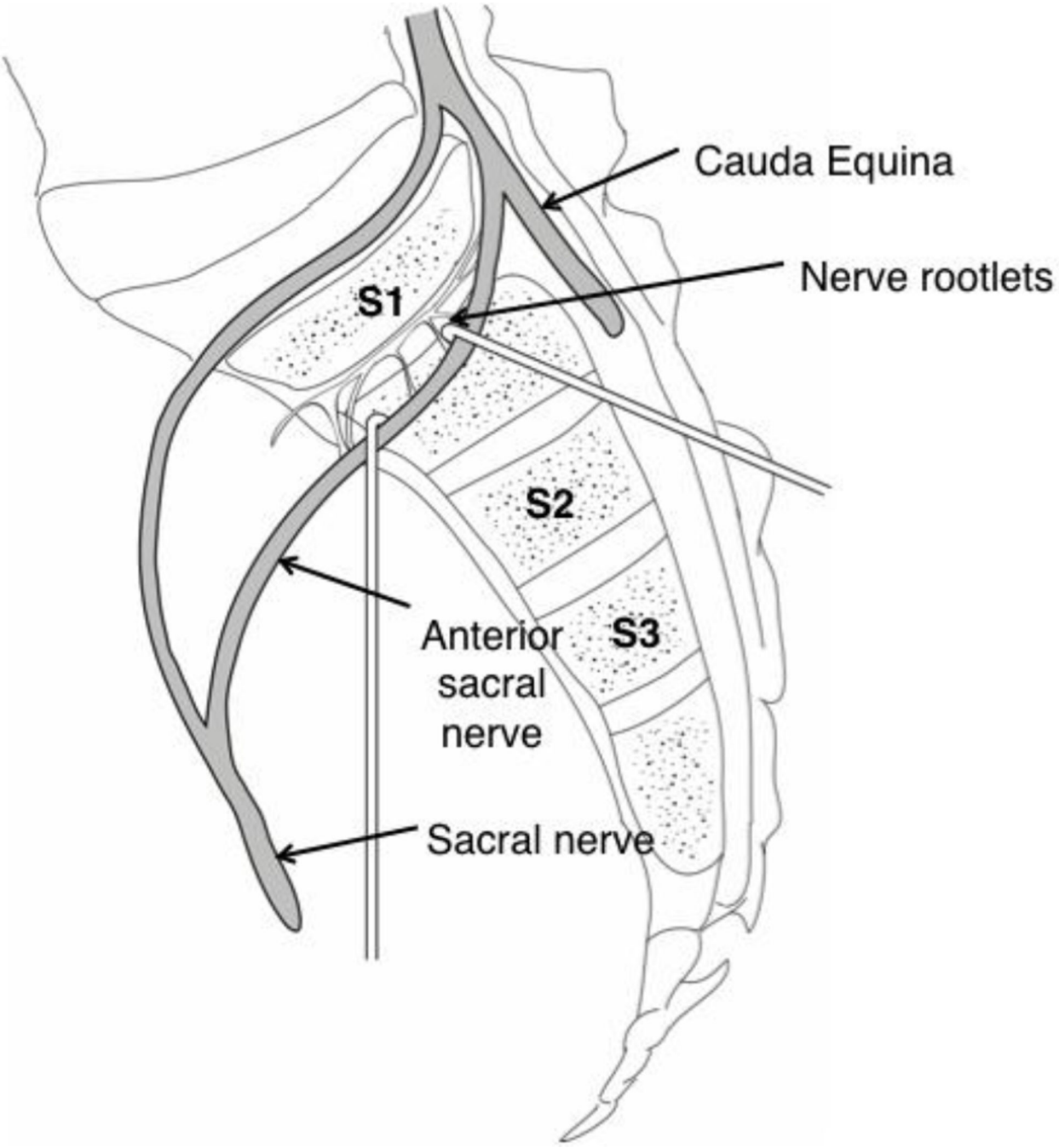

Figure 7.

Depicts a right parasagittal section through the sacrum demonstrating the anatomic and neural architecture observed during gross dissection. The S1 anterior sacral nerve demonstrates medial branching of small coursing fibers before other sacral and lower lumbar nerves join to form distal neural structures of the lower limb.